Supplemental Material for the article "Constraints on the dipole photon strength for the odd uranium isotopes"

(Dated: February 4, 2022)

In order to keep the length of the paper reasonable, we decided to include a reduced number of figures with only specific and representative examples comparing experimental and simulated spectra. In this Supplemental Material many more comparisons are given.

I. EXPERIMENTAL SPECTRA

Experimental sum-energy and MSC spectra for resonances used in our analysis are shown in Figs. 1-3 for ^{234}U, ^{236}U and ^{238}U, respectively. the figure for ^{234}U is identical to Fig. 4 of the paper.

II. FORMULAE FOR TESTED MODELS

To avoid any ambiguity we list here explicit formulae for a few models used in the paper. With index i we indicate that there could be several contributing resonance terms; E_γ then denotes γ-ray energy.

The Standard Lorentzian (SLO) form (used for description of $M1$ resonance terms) is

$$\mathrm{SLO} = \sum_i \frac{\sigma_i \Gamma_i}{3(\pi\hbar c)^2} \frac{E_\gamma \Gamma_i}{(E_\gamma^2 - E_i^2)^2 + E_\gamma^2 \Gamma_i^2}. \quad (1)$$

The enhanced generalized Lorentzian model, EGLO(k,T), has the form

$$\mathrm{EGLO}(k,T) = \sum_i \frac{\sigma_i \Gamma_i}{3(\pi\hbar c)^2} \left[\frac{E_\gamma \Gamma_i(E_\gamma,k,T)}{(E_\gamma^2 - E_i^2)^2 + E_\gamma^2 \Gamma_i^2(E_\gamma,k,T)} + 0.7\frac{\Gamma_i(0,k,T)}{E_i^3} \right], \quad (2)$$

with

$$\Gamma_i(E_\gamma,k,T) = \Gamma_i \frac{E_\gamma^2 + 4\pi^2T^2}{E_i^2} \left[k + (1-k)\frac{E_\gamma - E_\gamma^0}{E_i - E_\gamma^0} \right]. \quad (3)$$

The factor $E_\gamma^0 = 4.5$ MeV as proposed by Kopecky *et al.* [1] was always used.

The generalized Lorentzian (GLO) model mentioned in the paper corresponds to the EGLO with $k = 1$. The prescription for k in Ref. [2] gives k almost precisely equal to one and thus leads to reduction of EGLO to GLO for U isotopes.

The modified generalized Lorentzian model, MGLO(k,T), is then given by

$$\mathrm{MGLO}(k,T) = \sum_i \frac{\sigma_i \Gamma_i}{3(\pi\hbar c)^2} \left[\frac{E_\gamma \Gamma_i(E_\gamma,k,T)}{(E_\gamma^2 - E_i^2)^2 + E_\gamma^2 \Gamma_i^2(E_\gamma,k,T)} + 0.7\frac{\Gamma_i(0,1,T)}{E_i^3} \right], \quad (4)$$

and evaluating the second term for $E_\gamma = 0$ and $k = 1$ leads to $0.7\,\Gamma_i\,4\pi^2T^2/E_i^5$. The difference between EGLO and MGLO is only in the second term on the right-hand-side of Eqs. (2) and (4), which describes the behavior at low γ-ray energies. The low-energy enhancement is, for given k, significantly smaller for the MGLO model.

The enhanced Lorentzian (ELO) model can be obtained from Eqs. (2) or (4) by neglecting the second term on the right-hand-side and setting $k = 1$, which yields

$$\mathrm{ELO}(T) = \sum_i \frac{\sigma_i \Gamma_i}{3(\pi\hbar c)^2} \left[\frac{E_\gamma \Gamma_i(E_\gamma,1,T)}{(E_\gamma^2 - E_i^2)^2 + E_\gamma^2 \Gamma_i^2(E_\gamma,1,T)} \right]. \quad (5)$$

Two different treatments of temperature T were considered in simulations with the MGLO and EGLO models – (i) $T = const$, or (ii) $T = T(E) \equiv \sqrt{(E_f - \Delta)/a}$, where E_f is the excitation energy of a final level, a the shell-model NLD parameter, and Δ the pairing energy. Only the second option was used for the ELO model. The values of a were adopted from Ref. [3], specifically $a = 25.08$, 23.22, 26.67 MeV^{-1} for ^{235,7,9}U, respectively. The values of Δ then correspond to the deuteron pairing energy as given in Ref. [4], specifically $\Delta = 0.261$, 0.428, 0.376 MeV for ^{235,7,9}U, respectively.

Tab. I lists parameters of PSF resonance terms corresponding to models compared in figures in this Supplemental Material.

III. COMPARISON OF EXPERIMENTAL SPECTRA TO SIMULATIONS

A. Model combinations from literature

Comparison of models available in the literature with experimental spectra can be found in Fig. 4. The panel for ^{234}U(n,γ) is identical to Fig. 8 in the article.

B. Search for optimal PSFs

As mentioned in the paper, similarly good agreement between experiment and simulations can be reached using different parameters of PSFs, in particular different k of the MGLO $E1$ model in conjunction with adjusted SC parameters. The paper shows a comparison for the MGLO model with $k = 1.8$ and fixed $T = 0.3$ MeV.

The comparisons for the $T = 0.3$ MeV with $k = 2.5$ and 3.0 are visualized in Figs. 5 and 6, respectively. Figures 7, 8 and 9 then show the MGLO model with $T(E)$ dependent on excitation energy and with $k = 1.8, 2.5$ and 3.0, respectively.

In addition, simulations using ELO with energy-dependent temperature and EGLO model with $k = 1.8$ and $T = 0.3$ MeV in combination with both CT and BSFG NLDs are shown in Figs. 10 and 11, respectively. We found that ELO and EGLO models result in a better agreement when used in combination with BSFG and CT NLD, respectively. The parameters of $M1$ PSF coupled with the EGLO model are the same as for MGLO with $k = 2.5$ and $T(E)$, because the $E1$ PSFs behave similarly; for parameters see Tab. I.

C. Check of Scissors mode properties

Figures 12-14 compare experimental and simulated spectra with double- and single-resonance SC for the three isotopes, respectively. The parameters used for the single-resonance SC are $E = 2.45$ MeV, $\Gamma = 1.25$ MeV, and $\sigma = 1.20$ mb.

Figures 15-17 show predictions of models where we removed one of the two-resonance terms of the SC.

Figure 18 shows simulations where the double-resonance structure (called SC above) is moved to $E1$ PSF; $M1$ PSF consists only of the SF mode. Note that for this case we did not try to adjust the "SC" resonances parameters.

D. Comparison of multiplicity distribution

Figs. 19 to 23 compare the multiplicity distribution, which corresponds to events with $E_s = 5.0 - 5.6$ MeV, $4.9 - 5.3$ MeV, and $4.5 - 4.8$ MeV for ^{234}U, ^{236}U and ^{238}U samples, respectively. These are the same E_s energies as used for the construction of MSC spectra. Spectra from each resonance and each artificial nucleus from simulations were normalized to have sum of probabilities for $m = 1 - 8$ equal to unity. The uncertainties (mean plus/minus one sigma) correspond to the standard deviation of individual values. The simulations reproduce with reasonable precision the multiplicity distribution except for combinations ELO-CT, see Fig. 21 (bottom), EGLO-BSFG, see Fig. 22 (top), and RIPL-3, see Fig. 23.

IV. TOTAL RADIATIVE WIDTH

Total radiative widths simulated with presented model combinations are listed in Table II – an extended version of the corresponding Table III from the paper.

TABLE I. Extended version of Table II of the paper with parameters of PSF models used in simulations. The $E1$ PSF parameters correspond to the double-peaked GEDR energy E, width Γ and maximum cross section σ. The same quantities then characterize the double-peaked SC and the SF resonances in the $M1$ PSF. The MGLO and EGLO models are used with $T = 0.3$ MeV unless specified otherwise.

	$E1$ PSF						$M1$ PSF								
Model combination	E (MeV)	Γ (MeV)	σ (mb)	E (MeV)	Γ (MeV)	σ (mb)	E (MeV)	Γ (MeV)	σ (mb)	E (MeV)	Γ (MeV)	σ (mb)	$E^{\S}$ (MeV)	$\Gamma^{\S}$ (MeV)	σ (mb)
RIPL-3 [2]	11.11	1.12	243.3	13.41	4.98	426							6.61	4.00	2.35
Oslo*,†[5]	11.40	4.20	572	14.40	4.20	1040	2.15	0.80	0.45	2.90	0.60	0.40	6.61	4.00	7.00
Oslo*,‡[5]	11.40	4.20	572	14.40	4.20	1040	2.00	0.80	0.40	2.80	1.20	0.30	6.61	4.00	7.00
DANCE [6]	11.28	2.48	325	13.73	4.25	384	2.15	0.80	0.60	2.90	0.60	0.53	6.61	4.00	1.50
MGLO(1.8)	10.90	2.30	358.0	13.96	4.75	459.0	2.15	0.80	0.98	2.90	0.60	0.82	6.61	4.00	3.05
MGLO(2.5)	10.90	2.30	338.0	13.96	4.75	490.0	2.15	0.82	1.07	2.90	0.65	1.04	6.61	4.00	3.45
MGLO(3.0)	10.90	2.30	328.0	13.96	4.75	519.0	2.15	0.95	1.30	2.90	0.89	1.25	6.61	4.00	3.95
MGLO(1.8,$T(E)$)	11.00	2.50	399.0	14.11	4.22	452.0	2.15	0.70	0.78	2.90	0.80	0.98	6.61	4.00	2.50
MGLO(2.5,$T(E)$)	10.85	1.94	315.0	13.85	4.86	517.0	2.15	0.70	0.90	2.90	0.80	1.21	6.61	4.00	2.85
MGLO(3.0,$T(E)$)	10.93	2.09	324.0	14.06	4.74	542.0	2.15	0.70	0.88	2.90	0.80	1.28	6.61	4.00	3.10
ELO($T(E)$)	10.90	2.30	398.0	14.16	5.15	409.0	2.15	0.80	0.25	2.90	0.60	0.30	6.61	4.00	1.25
EGLO(1.8)	10.90	2.30	358.0	13.96	4.75	459.0	2.15	0.70	0.90	2.90	0.80	1.21	6.61	4.00	2.85

* $E1$ PSF contained an additional Lorentzian at 7.3 MeV with width of 2 MeV and maximum cross section of 15 mb;
† ^{235,237}U; ‡ ^{239}U; § the value was taken from systematic in RIPL-3 database [2] and was not adjusted

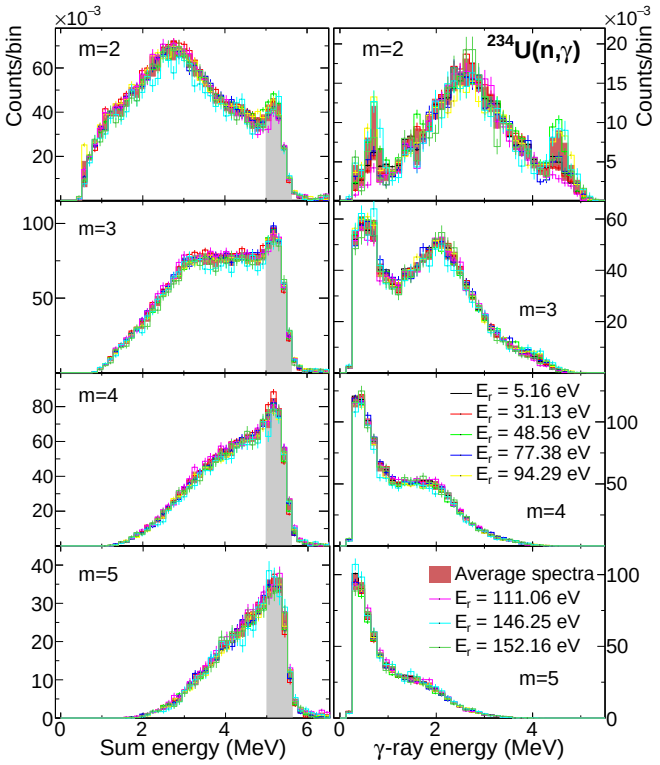

FIG. 1. The sum-energy (left column) and MSC spectra (right column) for individual resonances and multiplicities $m = 2-5$ after background subtraction for $^{234}\mathrm{U}(n,\gamma)$. The "average spectra" band represents the average of resonances plus minus one standard deviation representing the fluctuation among the resonances. The gray region in sum-energy spectra gives the range used in MSC and multiplicity spectra construction.

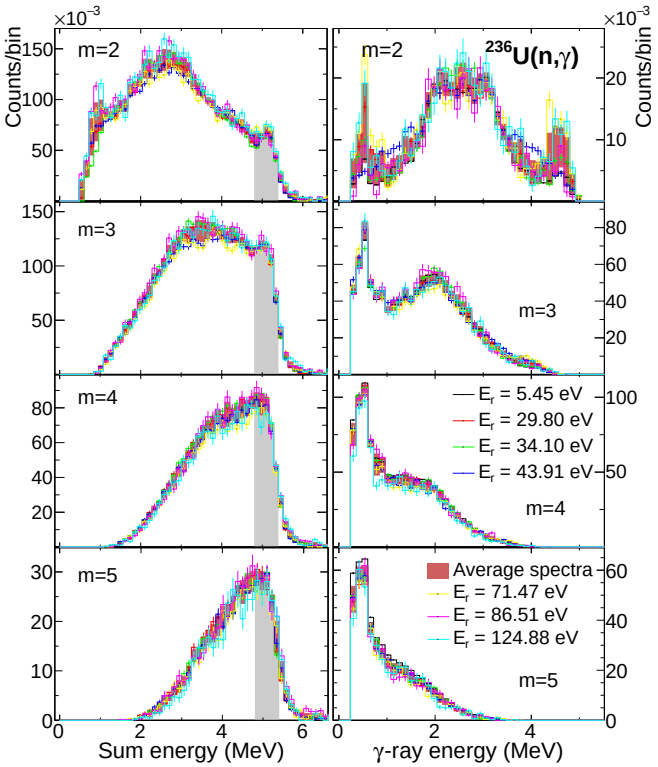

FIG. 2. The same as Fig. 1 but for $^{236}\mathrm{U}(n,\gamma)$.

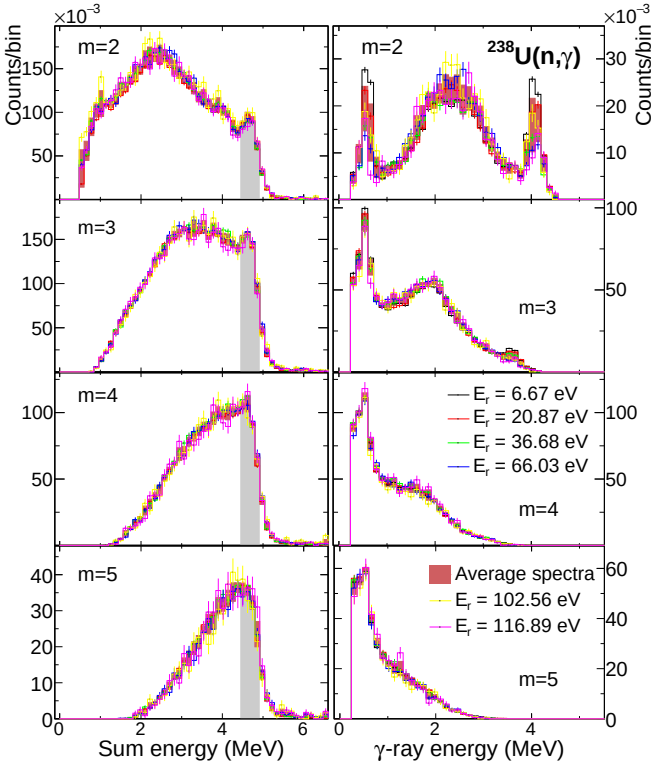

FIG. 3. The same as Fig. 1 but for $^{238}\mathrm{U}(n,\gamma)$.

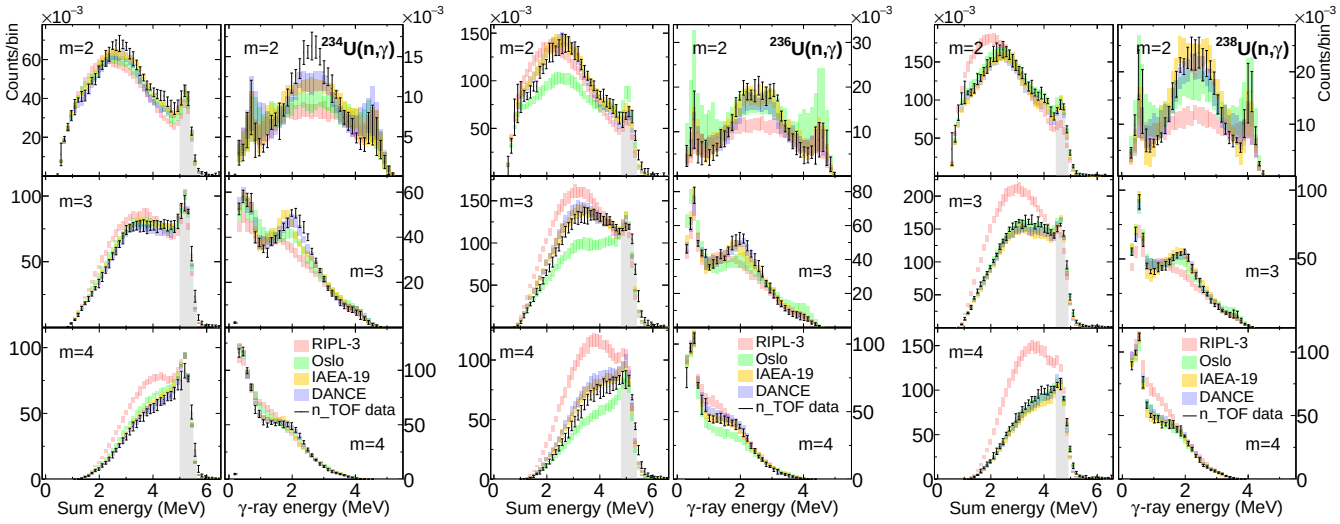

FIG. 4. Comparison of ^{234,236,238}U(n,γ) sum-energy (left columns) and MSC (right columns) spectra using model combinations RIPL-3, IAEA-19, Oslo, and DANCE.

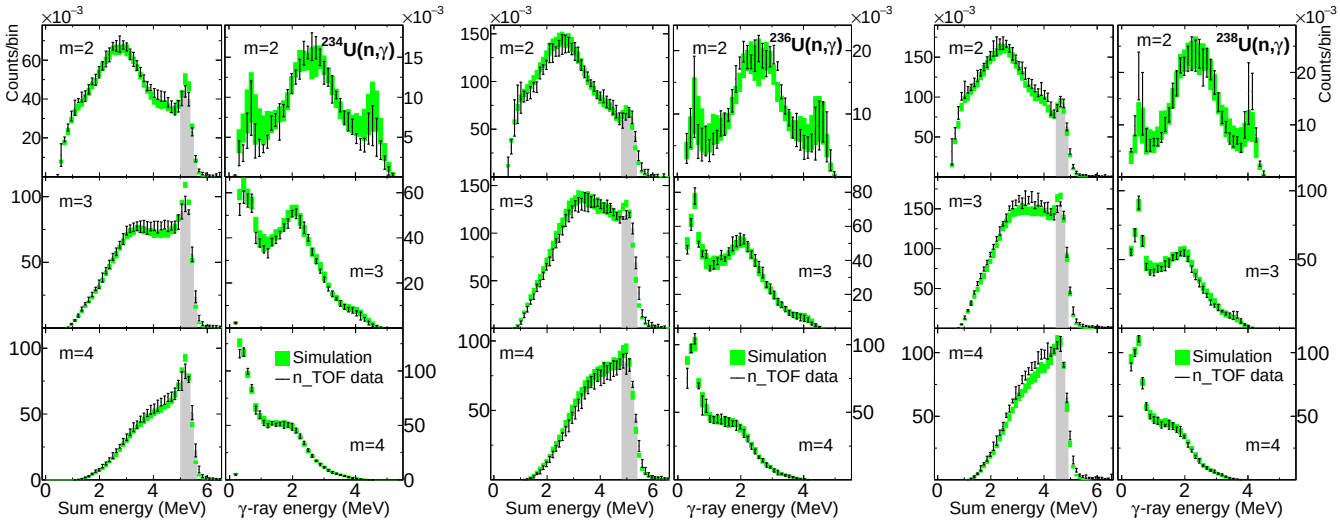

FIG. 5. Comparison of experimental and simulated sum-energy (left columns) and MSC spectra (right columns) for all three nuclei with the MGLO(2.5) model.

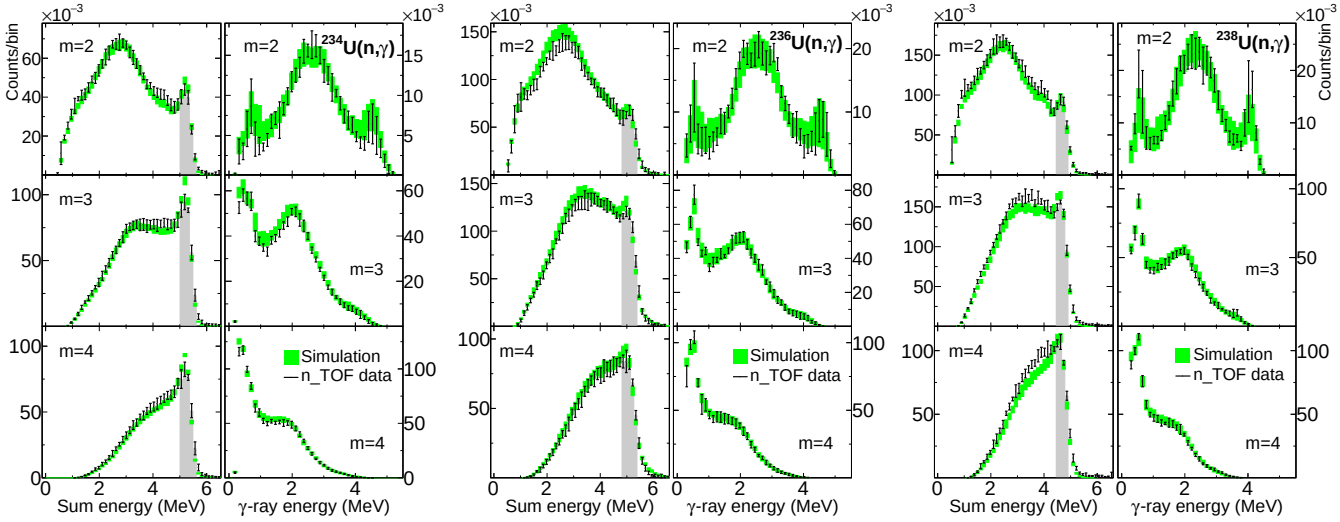

FIG. 6. The same as Fig. 5 but for MGLO(3.0) model.

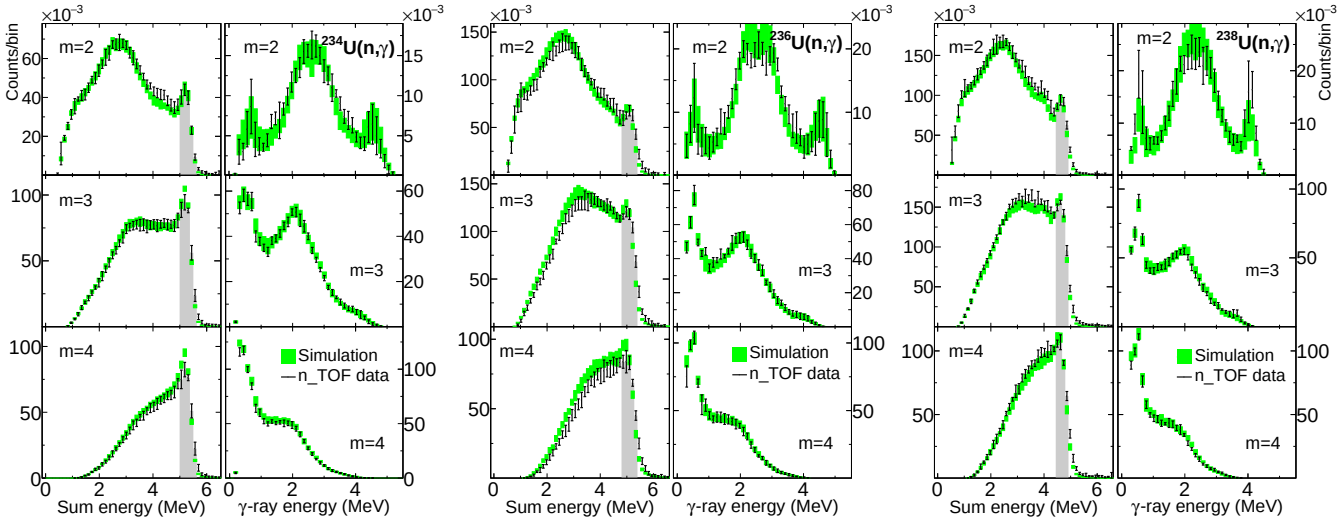

FIG. 7. The same as Fig. 5 but for MGLO (1.8,$T(E)$) model.

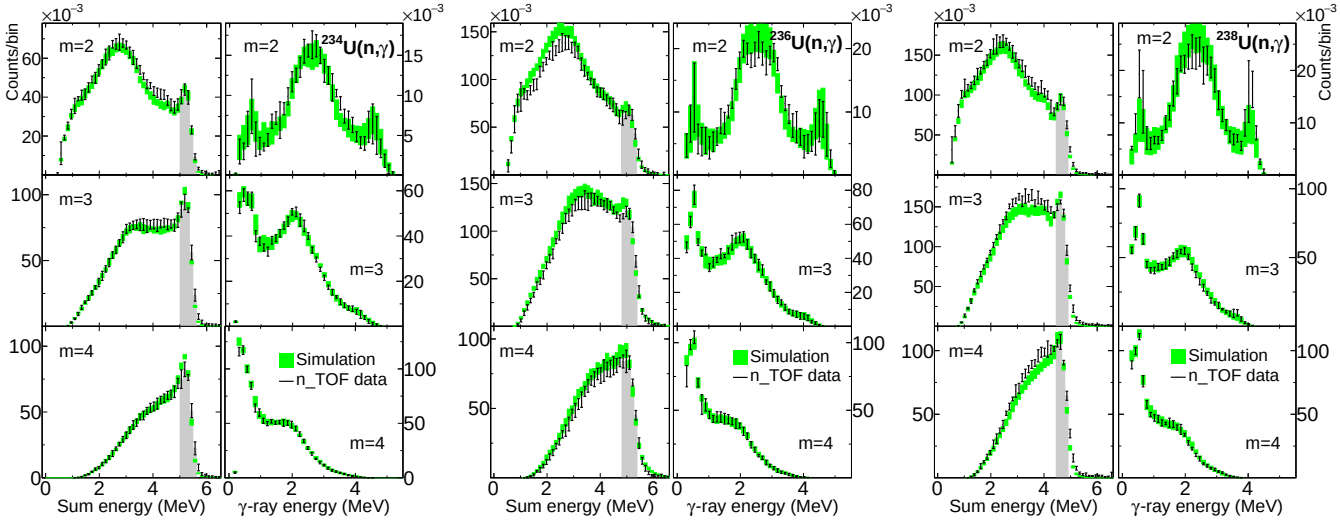

FIG. 8. The same as Fig. 5 but for MGLO(2.5,$T(E)$) model.

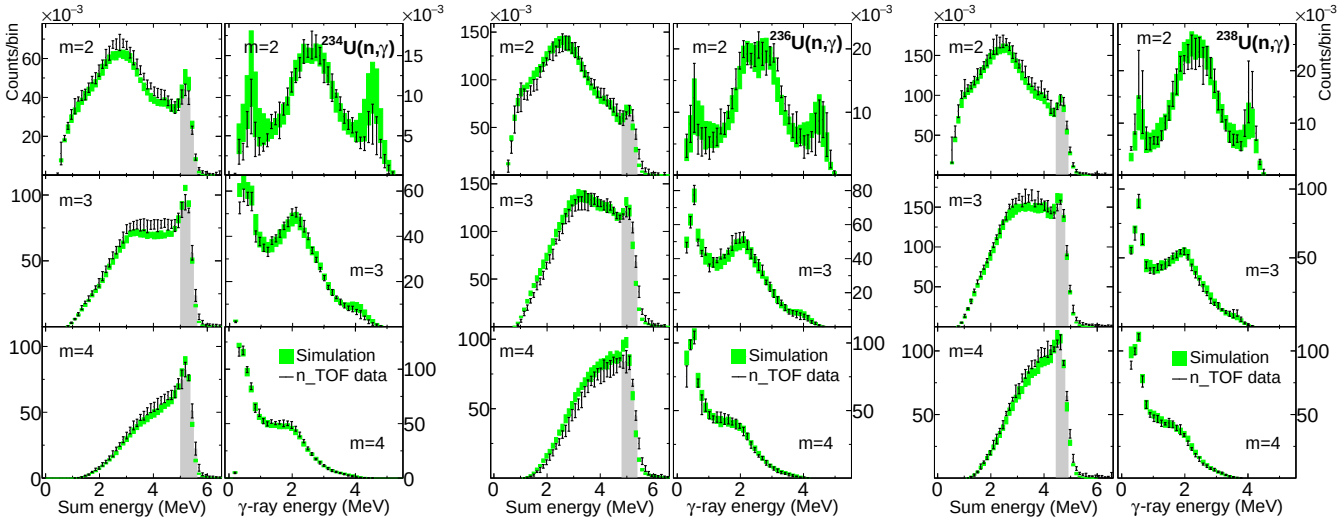

FIG. 9. The same as Fig. 5 but for MGLO(3.0,$T(E)$) model.

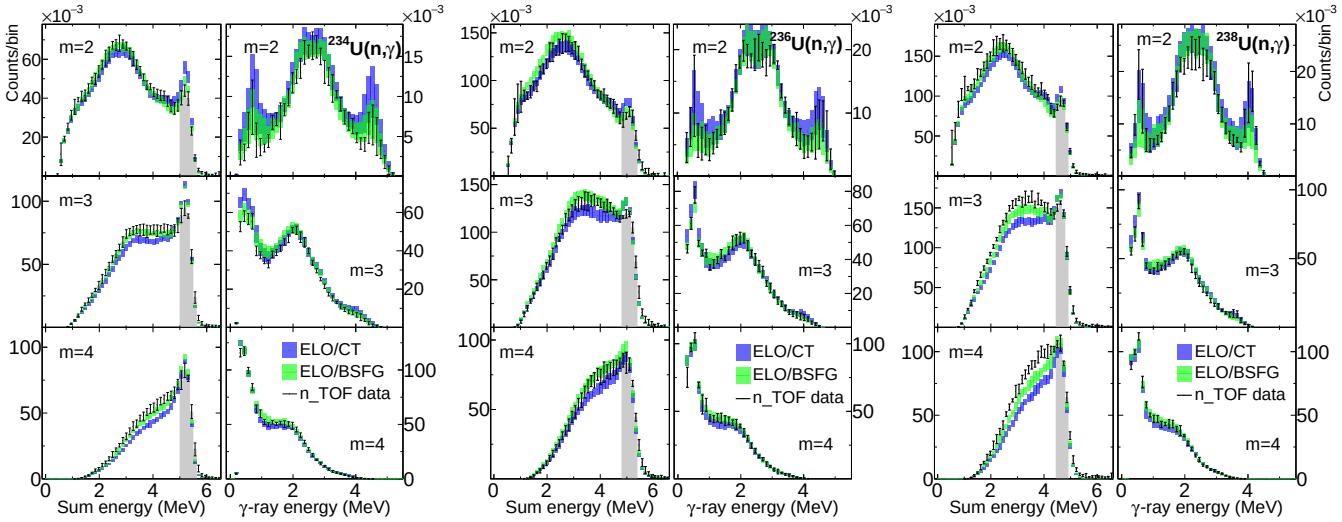

FIG. 10. The same as Fig. 5 but for ELO($T(E)$) $E1$ PSF model in combination with CT or BSFG NLD [4]. The legend shows the PSF/NLD model combination.

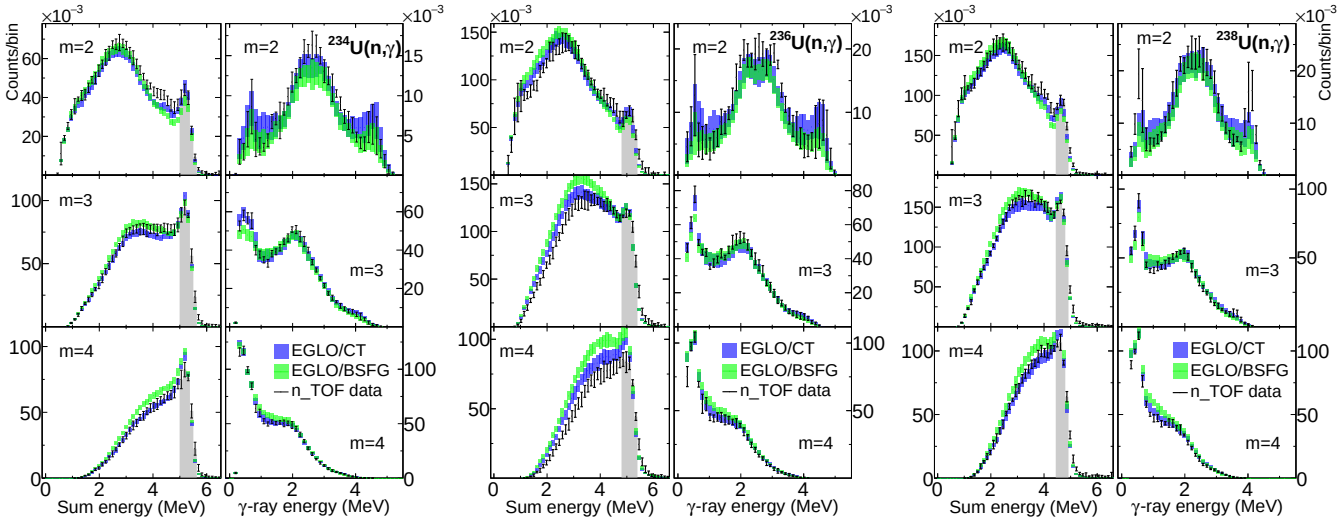

FIG. 11. The same as Fig. 5 but for EGLO(1.8) $E1$ PSF model in combination with CT or BSFG NLD [4]. The legend shows the PSF/NLD model combination.

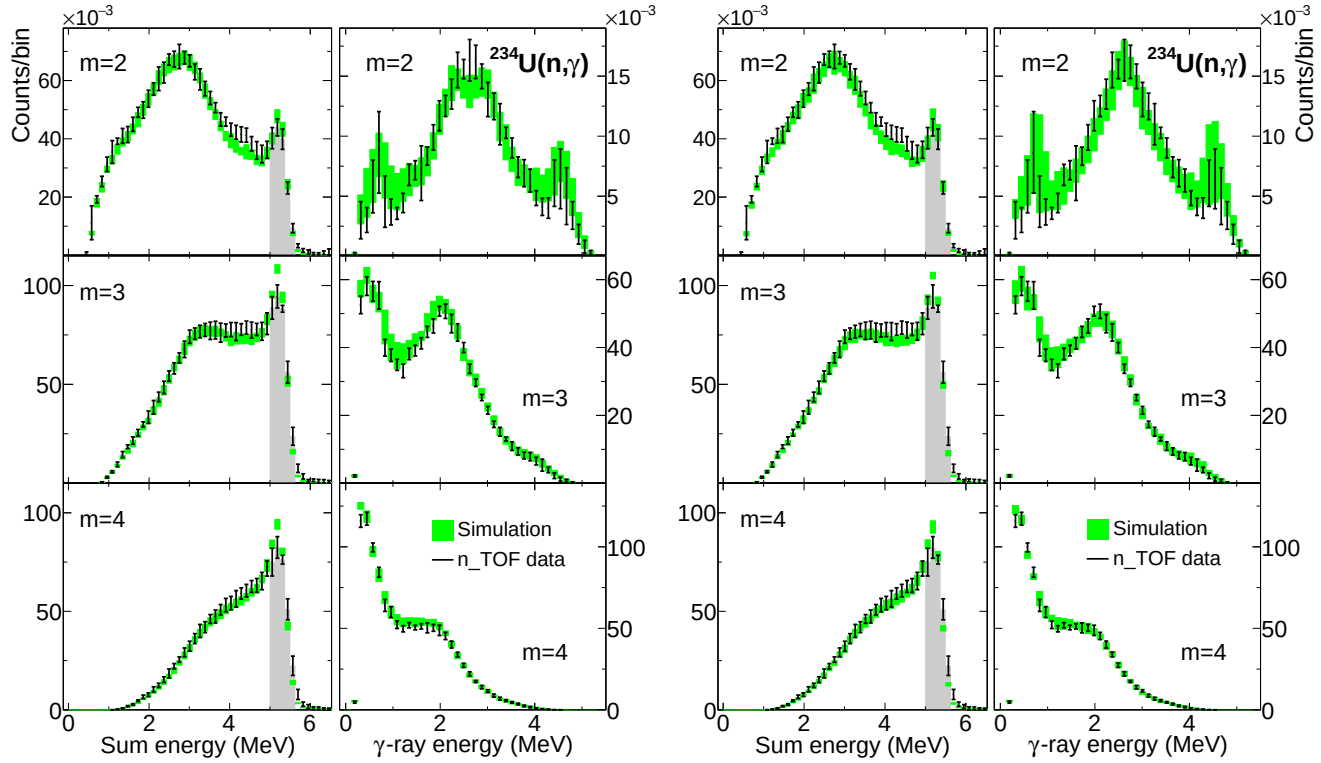

FIG. 12. Comparison of $^{234}\mathrm{U}(n,\gamma)$ sum-energy (left columns) and MSC (right columns) spectra with MGLO(1.8), in combination with the double-resonance (left) or single-resonance (right) SC.

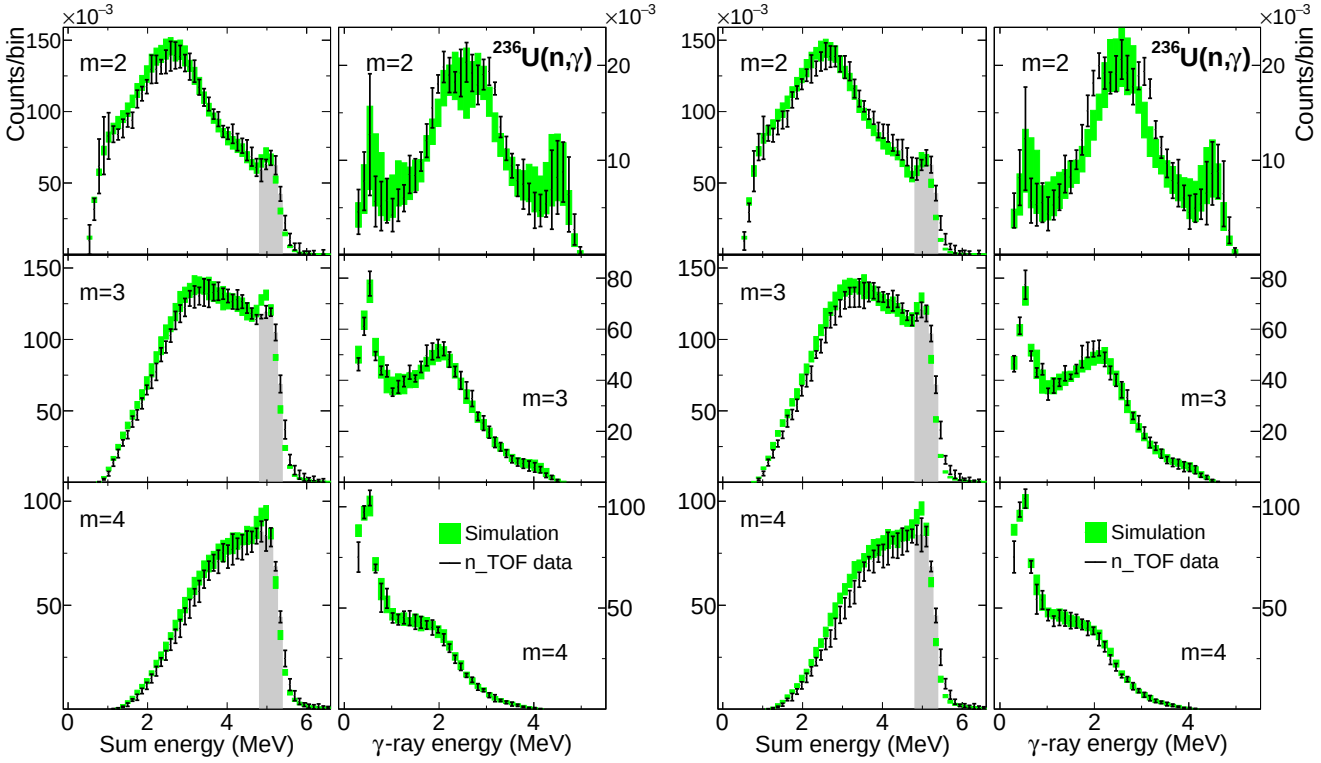

FIG. 13. The same as Fig. 12 but for $^{236}\mathrm{U}(n,\gamma)$ and MGLO(2.5) model.

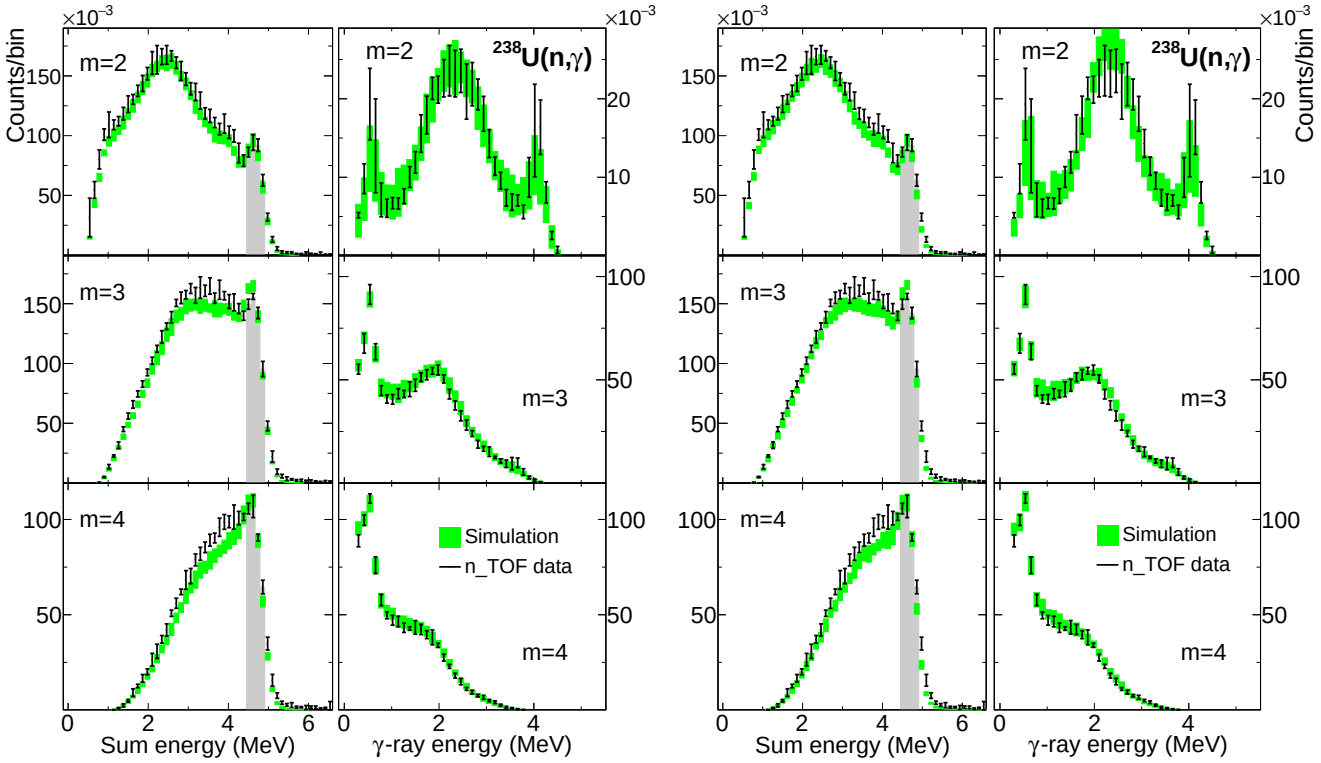

FIG. 14. The same as Fig. 12 but for ^{238}U(n,γ) and MGLO(3.0) model.

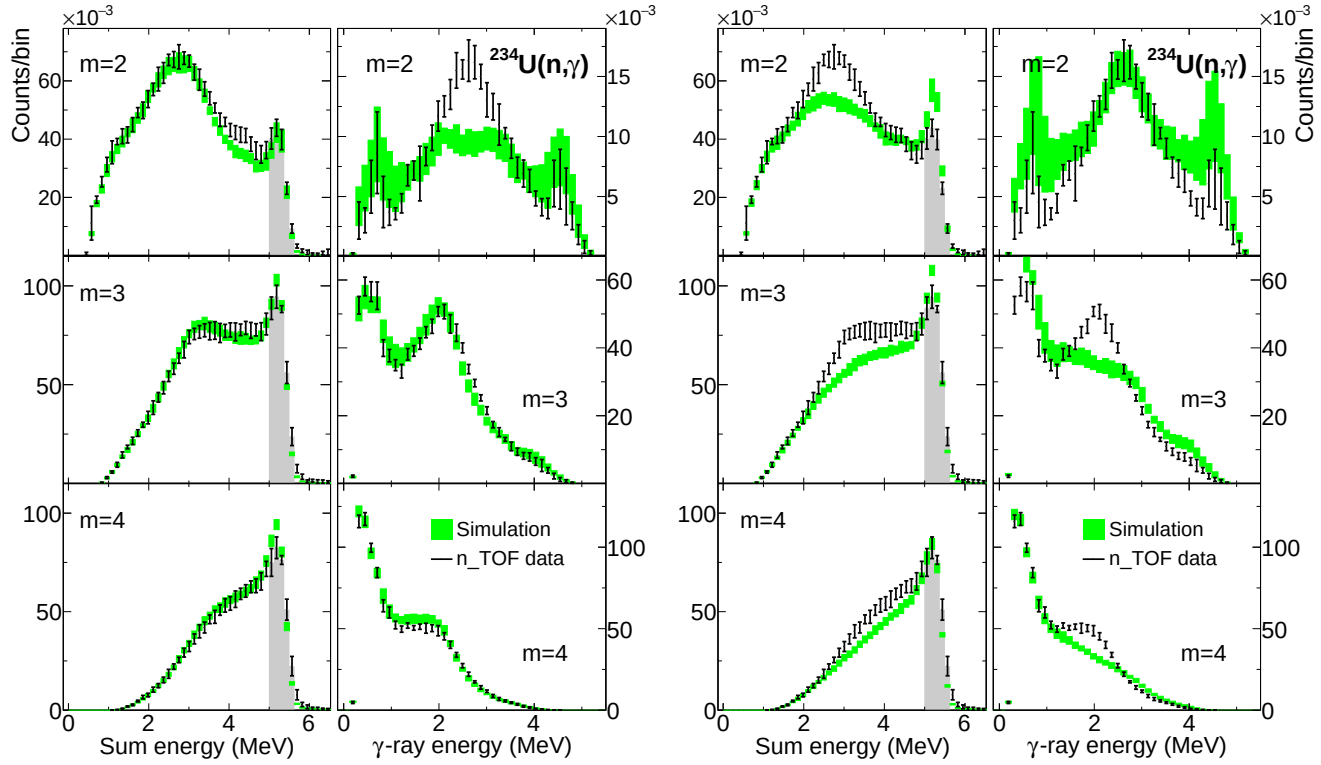

FIG. 15. Comparison of ^{234}U(n,γ) sum-energy (left columns) and MSC (right columns) spectra with MGLO(1.8) when higher-energy SC (left) and lower-energy SC (right) were removed.

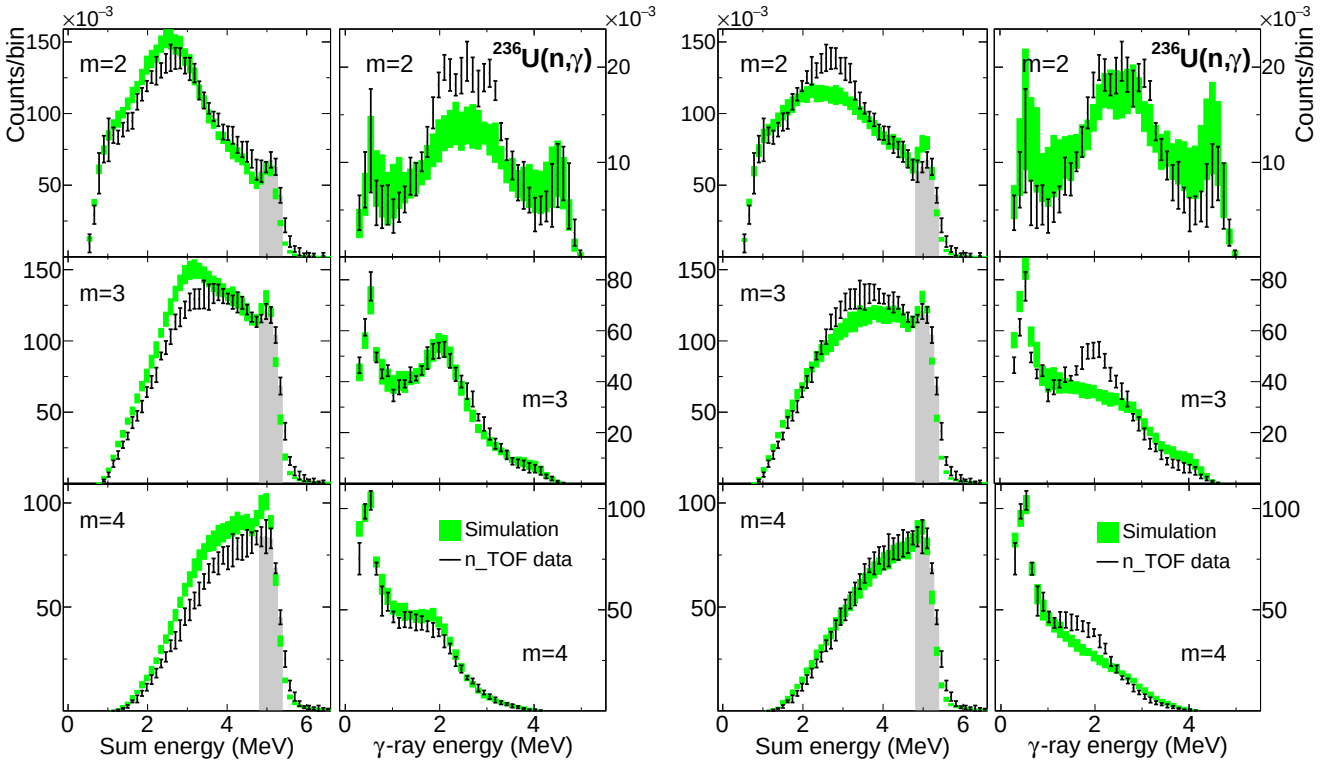

FIG. 16. The same as Fig. 15 but for $^{236}\mathrm{U}(n,\gamma)$.

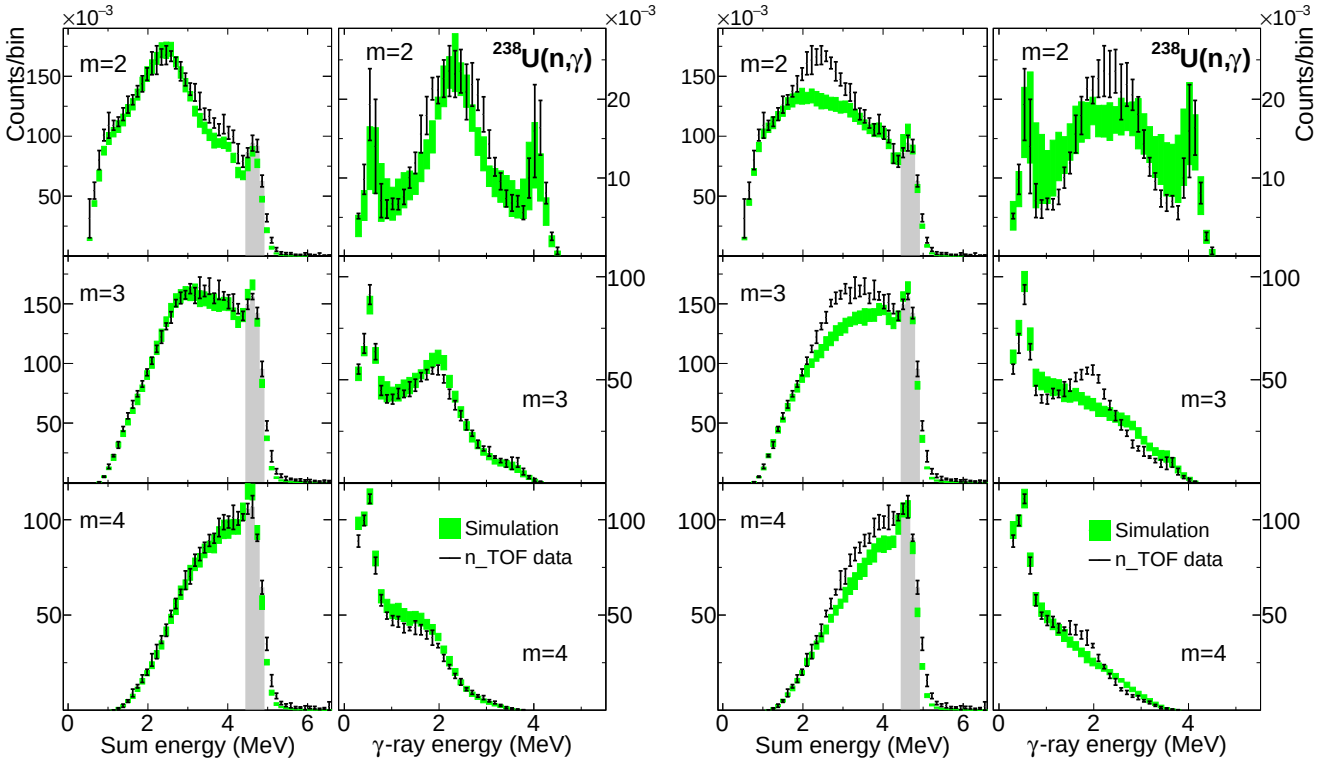

FIG. 17. The same as Fig. 15 but for $^{238}\mathrm{U}(n,\gamma)$.

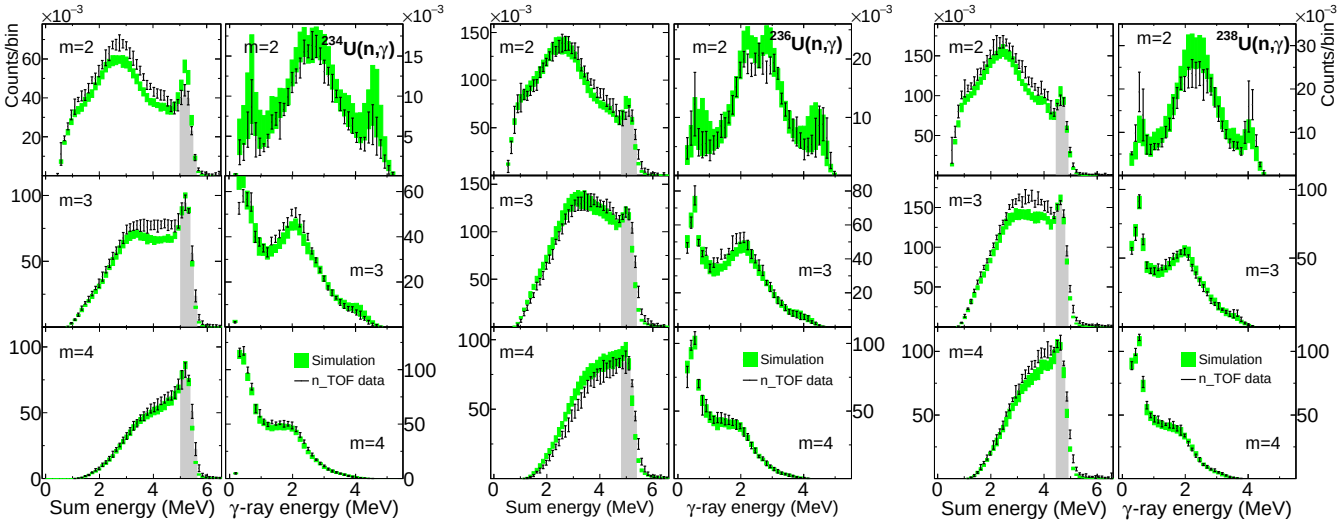

FIG. 18. Comparison of experimental and simulated sum-energy (left columns) and MSC (right columns) spectra for all three nuclei with double-resonance "SC" term considered to be of $E1$ character. The GEDR tail was described by MGLO model with $k = 1.8$ and $T = 0.3$ MeV for all three isotopes. The CT NLD model was used with respective parameters from Ref. [4].

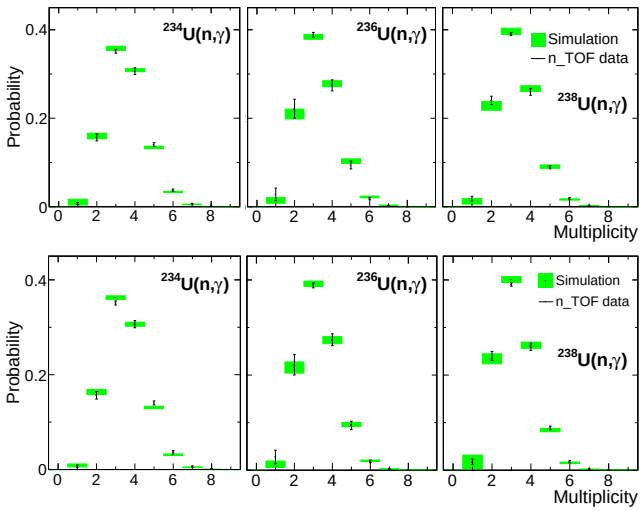

FIG. 19. Comparison of multiplicity distribution between experiment and MGLO(1.8) (top) and MGLO(3.0) (bottom) model combinations.

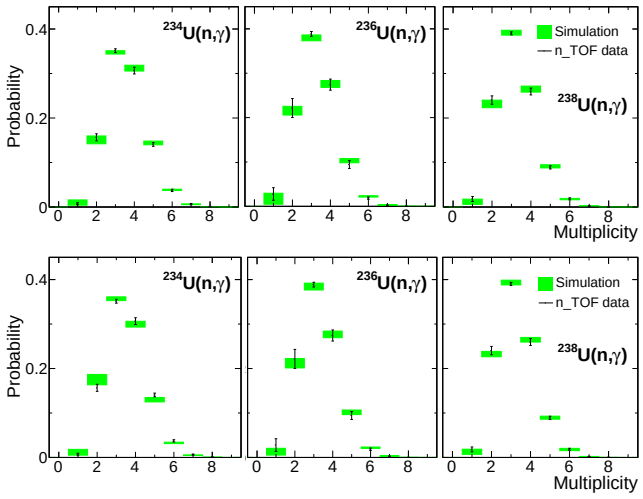

FIG. 20. The same as Fig. 19 but for MGLO(1.8,$T(E)$) (top) and MGLO (3.0,$T(E)$) (bottom) model combinations.

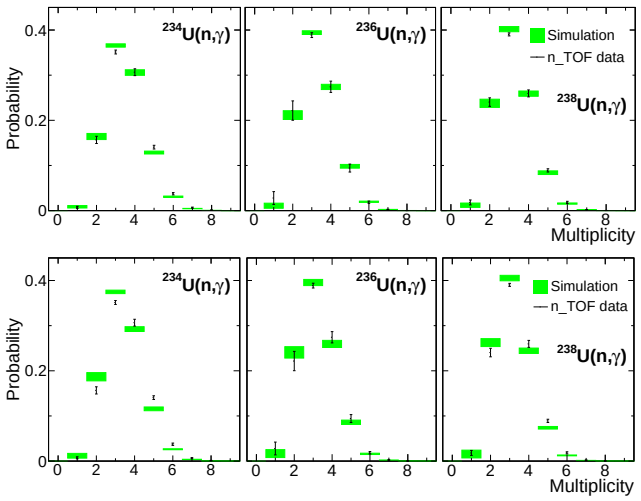

FIG. 21. The same as Fig. 19 but for ELO($T(E)$)-BSFG (top) and ELO($T(E)$)-CT (bottom) model combinations.

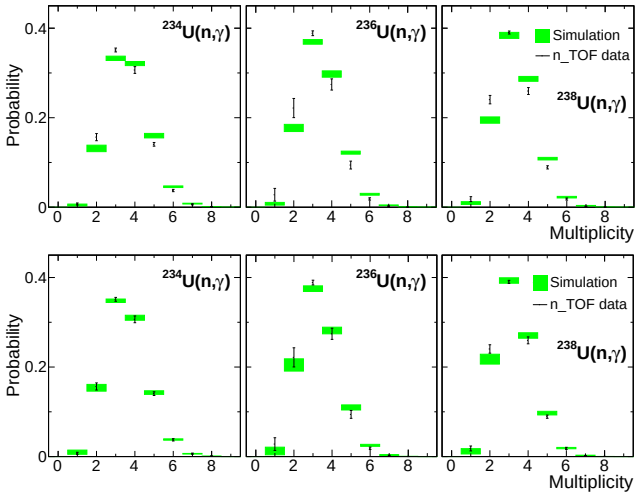

FIG. 22. The same as Fig. 19 but for EGLO(1.8)-BSFG (top) and EGLO(1.8)-CT (bottom) model combinations.

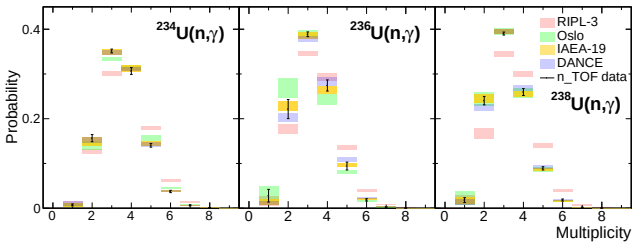

FIG. 23. The same as Fig. 19 but for model combinations RIPL-3, IAEA-19, Oslo and DANCE, i.e. those available in the literature.

TABLE II. Extended version of Tab. III from the paper. Total radiative widths Γ_γ of s-wave resonances obtained with different model combinations. The MGLO and EGLO model have a constant temperature of $T = 0.3$ MeV unless specified otherwise. The NLD model labels VE05 and VE09 correspond to Refs. [3] and [4], respectively.

Model combination PSF-LD	Γ_γ (meV) ^{234}U(n,γ)	^{236}U(n,γ)	^{238}U(n,γ)
RIPL-3	16.1(2)	12.9(2)	9.5(2)
IAEA-19	29.4(6)	19.3(5)	13.9(5)
Oslo	19.9(4)	20.4(6)	18.6(8)
DANCE	22.0(5)	17.2(4)	15.9(6)
MGLO(1.8) CT VE05	26.9(9)	21.3(5)	18.8(5)
MGLO(1.8) CT VE09	25.4(7)	20.1(5)	15.9(6)
MGLO(1.8) BSFG VE05	51.1(9)	43.9(9)	32.3(9)
MGLO(1.8) BSFG VE09	52.9(12)	47.8(12)	34.2(9)
MGLO(2.5) CT VE09	30.5(10)	23.9(7)	18.8(7)
MGLO(3.0) CT VE05	41.4(15)	32.7(10)	28.7(8)
MGLO(3.0) CT VE09	39.0(12)	30.9(9)	24.3(9)
MGLO(1.8,$T(E)$) CT VE09	26.7(7)	20.3(5)	15.5(6)
MGLO(2.5,$T(E)$) CT VE09	31.5(8)	24.5(6)	17.3(6)
MGLO(3.0,$T(E)$) CT VE09	33.4(9)	25.9(7)	19.2(7)
ELO($T(E)$) CT VE09	7.9(2)	5.9(2)	4.4(1)
ELO($T(E)$) BSFG VE09	16.7(2)	14.2(2)	9.7(3)
EGLO(1.8) CT VE09	31.7(9)	25.2(7)	19.8(8)
EGLO(1.8) BSFG VE09	65.7(14)	59.3(13)	42.6(13)
Mughabghab's atlas [7]	25.3(1)	23.4(8)	23.36(31)
Mughabghab's atlas [8]	36.7(7)	23.4(8)	22.9(4)
JEFF-3.3 [9, 10]	26.0	23.0	22.5
ENDF/B-VIII.0 [11]	26.0	19.5	22.5

[1] J. Kopecky, M. Uhl, and R. E. Chrien, Phys. Rev. C **47**, 312 (1993).

[2] R. Capote, M. Herman, P. Obložinský, P. G. Young, S. Goriely, T. Belgya, A. V. Ignatyuk, A. J. Koning, S. Hilaire, V. A. Plujko, M. Avrigeanu, O. Bersillon, M. B. Chadwick, T. Fukahori, Z. Ge, Y. Han, S. Kailas, J. Kopecky, V. M. Maslov, G. Reffo, M. Sin, E. S. Soukhovitskii, and P. Talou, Nucl. Data Sheets **110**, 3107 (2009).

[3] T. von Egidy and D. Bucurescu, Phys. Rev. C **72**, 044311 (2005), Erratum in Ref. [12].

[4] T. von Egidy and D. Bucurescu, Phys. Rev. C **80**, 054310 (2009).

[5] M. Guttormsen, L. A. Bernstein, A. Görgen, B. Jurado, S. Siem, M. Aiche, Q. Ducasse, F. Giacoppo, F. Gunsing, T. W. Hagen, A. C. Larsen, M. Lebois, B. Leniau, T. Renstrøm, S. J. Rose, T. G. Tornyi, G. M. Tveten, M. Wiedeking, and J. N. Wilson, Phys. Rev. C **89**, 014302 (2014).

[6] J. L. Ullmann, T. Kawano, B. Baramsai, T. A. Bredeweg, A. Couture, R. C. Haight, M. Jandel, J. M. O'Donnell, R. S. Rundberg, D. J. Vieira, J. B. Wilhelmy, M. Krtička, J. A. Becker, A. Chyzh, C. Y. Wu, and G. E. Mitchell, Phys. Rev. C **96**, 024627 (2017), Erratum in Ref. [13].

[7] S. F. Mughabghab, *Atlas of Neutron Resonances* (Elsevier, 2006).

[8] S. F. Mughabghab, *Atlas of Neutron Resonances* (Elsevier, 2018) Volume 2: Resonance Properties and Thermal Cross Sections Z= 61-102.

[9] A. J. Koning *et al.*, J. Korean Phys. Soc. **59**, 1057 (2011).

[10] A. J. M. Plompen *et al.*, Eur. Phys. J. A **56**, 181 (2020).

[11] D. A. Brown *et al.*, Nucl. Data Sheets **148**, 1 (2018), special Issue on Nuclear Reaction Data.

[12] T. von Egidy and D. Bucurescu, Phys. Rev. C **73**, 049901(E) (2006).

[13] J. L. Ullmann, T. Kawano, B. Baramsai, T. A. Bredeweg, A. Couture, R. C. Haight, M. Jandel, J. M. O'Donnell, R. S. Rundberg, D. J. Vieira, J. B. Wilhelmy, M. Krtička, J. A. Becker, A. Chyzh, C. Y. Wu, and G. E. Mitchell, Phys. Rev. C **104**, 019902(E) (2021).